Formation and structure of the Al–Mn–Pt "Robinson-type" phase

Susanna Syniakina[1], Benjamin Grushko[2], Louisa Meshi[1*]

[1] *Department of Materials Engineering, Ben Gurion University of the Negev, Beer Sheva, Israel*
[2] *Peter-Grünberg-Institut, Forschungszentrum Jülich, 52425 Jülich, Germany*

Abstract

The stable "Robinson-type" phase (R-phase, C*mcm*, a = 7.730 Å, b = 24.035 Å and c = 12.597 Å) was revealed at 700 °C in a small compositional region around $Al_{79.5}Mn_{16}Pt_{4.5}$. Partial phase equilibria in its vicinity were determined at 700 °C. At this temperature, it is in equilibrium with the ternary extension of the Al–Mn T-phase, whose compositional region propagates up to that of the R-phase. An atomic model of the R-phase, containing 124 Al, 24 Mn and 8 Pt atoms, was deduced using direct methods applied to the 3D electron-diffraction tomography data and compared to those of the Al–Mn–Ni R-phase and Al–Mn–Pt(Pd) T-phase.

Keywords: Al–Mn–Pt; Intermetallics; Phase diagrams; Crystal structure; 3DED; Electron crystallography.

1. Introduction

The Al–Mn–TM alloy systems (TM = Cr, Fe, Co, Ni, Cu, Pd, Pt) evoked a great interest due to the formation of complex intermetallics in their Al-rich compositional regions, particularly the so-called "Taylor phase" (T-phase, orthorhombic, a~14.7Å, b~12.6Å, c~12.5 Å) and "Robinson phase" (R-phase, orthorhombic, a~7.7Å, b~24Å, c~12.5Å), both containing pentagonal atomic arrangements, also typical of quasiperiodic structures (see Ref. [1] and references therein). Many papers were devoted to construction of phase diagrams of the Al-Mn-TM systems, structure evaluation of the T and R phases in the Al-Mn-TM alloys as well as on their structural relationship. In each system – specific structural features of these phases were found, therefore revealing T and/or R phases in a new system requires thorough crystallographic and metallurgical study as presented in current paper focusing on the R phase revealed in the Al-Mn-Pt system.

In the recent refinement of the Al–Mn–Pt phase diagram [1], previously studied in Ref. [2], the ternary compositional region of the binary orthorhombic Al–Mn T-phase was updated at 800 to 1100 °C and compared to the equivalent regions in other Al–Mn–(TM) systems (TM = Cr, Fe, Co, Ni, Cu, Pd). Particularly, the propagation of the T-phase region towards higher-Al was concluded up to the $Al_{78}Mn_{17.5}Pt_{4.5}$ composition. This study also revealed the formation of the nanometric plate-like inclusions inside the grains of the above-mentioned Al-rich T-phase annealed at 800 °C. They were asserted to the so-called R-phase, also known to coexist with the T-phase in the Al–Mn–Pd system (see [3] and references therein). The precipitation of the R-phase from a supersaturated T-phase matrix was supposed to take place during cooling from the annealing temperature. The space group variation in the Al–Mn–Pt T-phase, reported in [1] has been studied in more detail in [4]. These changes were associated with the compositional variations and not effected by the supersaturation of the T-phase or formation of the precipitates. On the other

* Corresponding author. E-mail: louisa@bgu.ac.il

hand, supersaturation could be a reason for the difficulties in the determination of the structural model of the T-phase, mentioned in [1].

The small size of the R-phase precipitates and their low fraction did not allow a study of their atomic structure in previous research. Considering the possible stability of the precipitated phase at lower temperature, the relevant alloys were annealed at 700 °C. Investigation of these alloys confirmed the structural similarity of the precipitates to the Al–Mn–Pd R-phase and the thermodynamic stability of both R and T in the Al–Mn–Pt alloy system at this temperature. The corresponding region of the 700 °C isothermal section of Al–Mn–Pt was constructed.

Investigation of the alloys annealed at 700 °C allowed the determination of the structural model of the R-phase with very close composition to that of the T-phase. The model was deduced using direct methods applied to the 3D electron-diffraction (3DED) tomography data, and the arrangement of the heavy atoms was compared to that of the T- phase reported in [1]. The structural model of the Al–Mn–Pt R-phase was also compared to that of the Al–Mn–Ni R-phase.

2. Experimental

The experiments were carried out on four alloys, whose compositions are marked in Fig. 1a. The purity of Al was 99.999 %, of Mn 99.99 %, of Pt 99.9 %. Alloys of ~2 g were produced by levitation induction melting in a water-cooled copper crucible under a pure Ar atmosphere. The samples were annealed at 700 °C under vacuum of $9x10^{-7}$ mBar for 984 h. The scanning electron microscopy (SEM, JEOL 840a equipped with EDAX Genesis 200 emission spectroscopy system) was carried out on polished unetched surfaces. Parts of the annealed alloys were crushed for powder XRD using mortar and pestle. The powder X-ray diffraction (XRD) examinations were carried out using Cu Kα1 radiation and an imaging plate (Huber G670, 2θ = 0-100°). The lattice parameters of the phases were refined using the commercial STOE software. For the transmission electron microscopy (TEM) analysis, the alloys were ground into powder using an agate mortar and pestle, dispersed in isopropanol, and stirred in the ultrasonic bath. This suspension was dropped on a carbon-coated Cu TEM grid. The samples were studied using the JEOL JEM-2100 TEM operating at 200 kV. The 3D ED tomography data collection was performed manually in the selected-area electron-diffraction (SAED) mode. Four datasets were gathered, each was taken from a different particle. The off-axis patterns were recorded at the constant tilt step of 1° in the range of +60° to –17° (first dataset); +55° to –29° (second dataset), +60° to +11° (third dataset) and +40° to –65° (fourth dataset) using a JEOL tomography TEM holder. The data were merged using the PETS 2.0 [5a] and Triple [5b] software. The structure solution was performed using Direct Methods (DMs) incorporated in the SIR2019 package [6]. The least-squares refinement was performed using the SHELXL97 program [7].

Scanning TEM (STEM) investigations were carried out on a JEOL JEM-2100F TEM operating at 200 kV equipped with the JED-2300T Energy Dispersive Spectrometer (EDS), scanning coils and GATAN 806 high-angle annular dark field (HAADF) detector. The HAADF images were processed using the Bragg filter in the commercial Digital Micrograph software (GATAN).

3. Results and discussion

3.1. Formation of the bulk R-phase and phase equilibria in its vicinity at 700 °C

The $Al_{78}Mn_{17.5}Pt_{4.5}$ alloy (#2) annealed at 800 °C and extensively studied in [1, 4] consisted of the essentially single T-phase, while the above-mentioned fine precipitates, albeit detected by electron microscopy, were invisible in the corresponding powder XRD patterns. However, after additional annealing of this alloy at 700 °C for 984 h its powder XRD pattern contained noticeable reflections of a second phase which coexisted with the parent T-phase. Due to a high degree of reflections overlapping, its reliable identification by powder XRD was not possible in this alloy. On the other hand, the same reflections were revealed in the powder XRD pattern of the $Al_{82}Mn_8Pt_{10}$ alloy (#1) also annealed at 700 °C, which did not contain the T-phase. They were asserted to the R-phase (see section *3.2*), suggested earlier following the examination of the above-mentioned precipitates. This identification was also confirmed by the subsequent TEM studies (see section *3.3*). In the alloy #1, annealed at 700 °C, the R-phase coexisted with the ternary extension of Al_4Pt (λ_{Pt}-phase) and the solidified liquid. For illustration, Fig. 2 shows a small 2θ range of the powder XRD patterns of the three above-mentioned samples, chosen so that it will not contain the reflections of the λ_{Pt}-phase.

Prolonged annealing at 700 °C and the morphology of the resulting grains of the R-phase[1], in contrast to its appearance in a form of fine precipitates during cooling from 800 °C [1], are in favor of its thermodynamic stability and its equilibrium formation temperature between 700 and 800 °C. The phase equilibria in the vicinity of the R-phase at 700 °C, deduced from the results of the SEM/EDX and powder XRD examinations of four alloys annealed for 984 h, are shown in Fig. 1a. The relevant crystallographic data are included in Table 1.

At 700 °C, the R-phase is formed in a small compositional region around ~$Al_{79.5}Mn_{16}Pt_{4.5}$. Its lattice parameters were refined from the XRD data of the alloy #1 suggesting the space group C*mcm* (63): a = 7.730(2) Å, b = 24.035(6) Å and c = 12.597(3) Å (average $\Delta(2\theta)$ = 0.016°, maximum $\Delta(2\theta)$ = 0.063°, FOM F(30) = 20.5 for the total 47 reflections not overlapping with those of λ_{Pt} and (Al)).

3.2. Phases R and T in the Al–Mn–TM (TM – transition metal) alloy systems – systematization and phase relationship

In contrast to Al–Mn–Pt system, Al–Mn–Pd alloys have been extensively studied since 1990s, particularly those containing the R and T phases (see [3, 8] and references therein). Although these phases were frequently observed together in a wide compositional region of the T-phase, including binary Al–Mn compositions, the stability of the Al–Mn–Pd R-phase has only been concluded in a small compositional region equivalent to that reported in the Al–Mn–Pt (see Fig. 1b).

Earlier, a stable R-phase was revealed in the Al–Mn–Cu system [9, 12]. On the other hand, the frequently quoted Al–Mn–Ni and Al–Mn–Zn R-phases, also reported in [9] and described in more detail in [10] and [11], respectively, were not confirmed in more recent studies (see [12a] and references therein). Thus, at the $Al_{60}Mn_{11}Ni_4$ composition, mentioned in [9], asserted as an *orthorhombic* R-phase, a *hexagonal* κ-phase (designated ζ in [12]: $P6_3/m$, a = 17.625 Å, c = 12.516 Å) has been revealed [13]. The obvious differences between these phases forming at the equivalent compositions in Al–Mn–Cu and Al–Mn–Ni systems have been illustrated in Fig. 3 of Ref. [12] comparing the experimental powder XRD data with XRD patterns calculated from the corresponding structural models. It should be stressed that in [13], the phases were also identified using electron diffraction taken from the corresponding single-phase particles. This is also worth

[1] In the alloy #1. In the alloy #2, the R-phase was not resolved by metallography from the T-phase.

noting, that the composition $Al_{31}Mn_6Ni_2$ ($Al_{79.5}Mn_{15.4}Ni_{5.1}$), as refined in [10] for the suggested in that reference R-phase, is far away from that of the ternary extension of the T-phase in Al–Mn–Ni, which does not propagate above ~75 at. % Al and ~2-3 at.% Ni [13]. Unfortunately, the knowledge on the Al–Mn–Zn alloy system is not sufficient for a liable conclusion.

Suggested in the literature binary $Al_{124}Mn_{32}$ stoichiometry of the R-phase is the same as that of the T-phase [1], which is outside their compositional regions of stability. Due to the existence of stable ternary T and R phases, it can be concluded that the replacement of Mn by TM=Pt, Pd or Cu stabilizes these phases. The amount of TM atoms which can participate in the T and R ternary phases depends on the TM atom type. For example, the total stability region of the Al–Mn–Cu R-phase is widely extended towards lower Al concentrations [1, 12] which is not the case in the Al–Mn–Pd and Al–Mn–Pt R phases, see Fig. 1c. In these systems, the stability regions of the R-phase are consistent with the replacement of exactly 8 Mn atoms by Pt or Pd at very specific positions, while the Al concentration remains as at the binary composition [3, 8 and this work]. In systems where TM=Cu, Pt or Pd, the R-phases, forming at lower temperatures, coexist with the ternary extensions of the Al–Mn T-phase at their Al-rich limits, and the total regions of the T and R phases could partially overlap. For TM=Pt, at the $Al_{78}Mn_{17.5}Pt_{4.5}$ composition, the R-phase is formed at 700 °C and the T-phase at 800 °C. The above-mentioned formation of the nanoscale R-phase precipitates inside the grains of the $Al_{78}Mn_{17.5}Pt_{4.5}$ T-phase, annealed at 800 °C, indicates some shrinkage of the Al-rich limit of the T-phase compositional region below 800 °C.

The close structural relationship between the R and T phases has been emphasized in numerous publications (see [3, 8, 15] and references therein). Thus, both structures can be presented as a staking of flat (or pseudo-flat) and puckered layers with the same total periodicity of ~12.5 Å [8, 15], where the same groups of atoms (pentagonal, particularly) are differently arranged. In the corresponding projections, the centers of the neighboring pentagons form regular hexagons expanded along their diagonals, as is illustrated in Fig. 3a for the R-phase according to Ref. [10]. These hexagons can be recognized due to the location of the heavy atoms (Fig. 3 a-d) exhibited the projections of the atomic columns in these phases along the *specific* orientation[2] according to the structural models of the $Al_{72.3}Mn_{24.5}Pd_{3.2}$ T-phase [15], $Al_{60}Mn_{11}M_4$ R-phase[3] [10] and $Al_{78}Mn_{17.5}Pt_{4.5}$ T-phase [1], respectively. Subsequently, the unit cells of both R and T contain the same total number of the 156 atomic positions [3, 8, 15 and this work], occupied depending on the composition. The theoretical relationship between their lattice parameters is: $c_R \approx c_T$, $b_R/a_T \approx b_T/a_R \approx \tau$ ($\tau = (1+\sqrt{5})/2 \approx 1.618$ is the golden mean). The lattice parameters of the $Al_{78}Mn_{17.5}Pt_{4.5}$ T-phase, coexisted with the R-phase were reported as: a = 14.720 Å, b = 12.628 Å and c = 12.545 Å [1]. Thus, the corresponding ratios $b_R/a_T = 1.633$ and $b_T/a_R = 1.634$ are indeed close to the golden mean.

The traces of the above-mentioned hexagons have also been recognized in the corresponding TEM lattice images of the relevant Al–Mn–Pd alloys (see [3, 15]). Similar patterns were also observed in the Al–Mn–Pt T and R phases. As can be clearly seen in Fig. 3 f and g, in both T and R the weaker spots, corresponding to the projections of the Mn columns, form the hexagons, while the stronger spots, corresponding to the projections of the Pt columns, locate inside the hexagons. These observations are consistent with the contrast in the HAADF images where the brighter spots are originated by the columns of the atoms with the higher atomic number. While such arrangements are consistent with the models of the T-phase in $Al_{72.3}Mn_{24.5}Pd_{3.2}$ [15] and $Al_{79.5}Mn_{16}Pt_{4.5}$ [1], this is not the case for the model of the R-phase of Ref. [10], where the positions

[2] This is [001] in the present work, in the literature this specific direction is frequently asserted to the b axis.

[3] To eliminate confusion in the following, we refer below to an Al–Mn–M R-phase.

inside the hexagons are occupied by Mn, while the Ni atoms (TM positions) were placed *at* the hexagons [10] (see Fig. 3 a and b).

In the more recent study of the Al–Mn–Cu R-phase [16], the positions of the TM atoms (TM=Cu in this case) have been also concluded to be inside the hexagons (model I in Ref. [16]), which is the same positions of the TM atoms revealed in our above-mentioned HAADF images of the Al–Mn–Pt R-phase (in our case TM=Pt). Although in Ref. [16] this was not noticeable in the corresponding HAADF images due to a low contrast between Cu and Mn, such an arrangement was revealed in their chemical mapping (see Fig. 6 presented in Ref. [16]). Earlier, similar positions of the TM atoms in the Al–Mn–Pd R-phase have been mentioned in Ref. [15] (TM was Pd in this case). These atoms are well seen in the TEM images inside the hexagons, due to a high contrast between Mn and Pd. Both these studies avoided applying these understandings and have not suggested structural changes to the structure of the accepted as a prototype Al–Mn–Ni R-phase of Ref. [10].

The model of Ref. [10] has been refined in Ref. [16] for studied there Al–Mn–Cu R-phase. The corresponding atomic parameters were obtained from "full relaxation of the structure model-I using first-principles calculations" [16]. Due to a higher content of Cu in the Al-Mn-Cu R phase ($Al_{20}Mn_3Cu_2$), relative to content of Ni in the Al-Mn-Ni R phase ($Al_{60}Mn_{11}Ni_4$), the additional Cu atoms completely replaced in Ref. [16] the Mn atoms at the 4*c* positions inside the hexagons. This TM-rich composition (in the case when TM is Cu) is somewhat outside the total compositional region of the R-phase, reported in Ref. [12b], but not very far from its higher Al limit at 550 °C (in this case, Al concentration decreases if Cu content increases). This should be mentioned, that in Ref. [16] the particles of the studied R-phase precipitated inside the (Al) matrix, which implies that R phase`s composition, in this case, correspond to the Al-rich limit of the R-phase region below the temperature of the Al–Cu eutectic (548 °C).

All these considerations underline the importance of the detailed structural study of each new R phase, as presented in the following chapter.

3.3. Structural characterization of the Al–Mn–Pt R-phase

Further investigation of the R-phase in TEM was carried out on four small fragments of the above-mentioned alloy #1 annealed at 700 °C. The methodology of the structure solution using 3D electron diffraction (3D ED) was documented numerously, for example [17]. In current research we have followed the steps listed in [18].

The completeness of the collected 3D ED datasets was 53.4%, 62.2%, 36.9% and 62.8%, respectively up to the resolution of 0.72 Å. The projections of the reconstructed reciprocal lattice along the highest symmetry axes taken from the fourth of the above-mentioned datasets (i.e., with highest completeness) are presented in Fig. 4. The cylindrical projections (not shown) of all datasets presented sharp peaks, indicating good reconstruction of the 3D reciprocal lattice and, thus, satisfactory data for the structure solution.

By merging these four datasets in the P1 space group, 87.5% data completeness was achieved up to the resolution of 0.72 Å. The reciprocal lattice cuts of the dataset are shown in Fig. 5. Analyzing these cuts the reflection conditions can be deduced. For example: h0l vs. h1l planes exhibit disappearance of lines of reflections pointing to the condition (*h0l*): $h, l = 2n$; in 0kl vs. 1kl a shift of the lines is observed, while in hk0 the rhombus pattern points to the (*hk0*): $h + k = 2n$ condition. Combining these and additional conditions which were deduced and comparing them

with extracted intensities from the merged dataset, the following extinction conditions were deduced: (*hkl*): $h + k = 2n$; (*0kl*): $k = 2n$; (*h0l*): h, $l = 2n$; (*hk0*): $h + k = 2n$; (*h00*): $h = 2n$; (*0k0*): $k = 2n$ and (*00l*): $l = 2n$. These extinction conditions are consistent with the C-c- extinction symbol [14]. Out of the three relevant space groups C*mc*2_1 (36), C2*cm* (40) and C*mcm* (63) [14], the latter was chosen due to its highest symmetry. This space group was also assigned by Robinson in Ref. [10] for the R-phase in other Al–Mn–M systems.

The structure solution was performed on the merged data containing 1635 independent reflections using direct methods utilized in SIR2019 software [6]. The solution contained all heavy atoms and some of the Al atoms, with a clear differentiation among the atom types, with the final residual value of 37.71%. In the Fourier difference space, the atomic positions exhibited the peaks with the heights related as 15:7:3 were asserted to Pt, Mn and Al, respectively. This partial atomic model underwent a kinematical least-squares refinement ($I \propto |F|^2$) vs. the 3D ED data in the ShelXL software [7]. The stability of the model (shift of the atom positions, interatomic distances, and the thermal motion parameters) was checked after each refinement cycle. Although at the final step some Al atoms still exhibited negative thermal motion parameters, the refinement was stable, and all atomic positions were refined (see Table 2). Although the reliability factor of the refinement $R_1 = 35.9$ % is high, the following comparison of the model to the corresponding HAADF images (see Fig. 3 e and g) and expected coordination polyhedra, as well as reasonable interatomic distances (shown in Table 3) gave confidence that the solution is correct. Due to noisy data of electron diffraction, refinement (especially if kinematical refinement is used on dynamical data) leads to quite high reliability figures. Many researchers have addressed this fact [1, 17-21]. This does not necessarily mean that the solution or refinement is wrong – it just requires additional validation as provided here.

The final model contained all 124 Al, 24 Mn and 8 Pt atoms, which is close to the $Al_{79.5}Mn_{16}Pt_{4.5}$ composition, measured by EDS. It should be noted that it is possible that there is some degree of disorder (partial occupancy of the Wyckoff sites), but in current research the occupancies were not refined. Furthermore, it is most likely that it would be impossible to use kinematical refinement against our data which was dynamical. Projection of the heavy atoms along [001] orientation is shown in Fig. 3 e.

The atomic coordinates in the presently developed model of the Al–Mn–Pt R-phase are quite close to those reported in Ref. [10] or Ref. [16] for the Al–Mn–M R-phase (see Table 4).

The arrangements of the heavy atoms in the structural model of the Al–Mn–Pt R-phase (this work) is compared in Fig. 3 to that of the Al–Mn–Pt T-phase of very close composition deduced independently in Ref. [1]. Although the T-phase model of Ref. [1] is not completed, it contains the positions of all heavy atoms: 24 Mn and 8 Pt. The flattened hexagons mentioned in section 3.2 are well recognized in both R and T (Fig. 3 a-e, respectively). They are arranged in parallel in the former and in the herringbone manner in the latter. This is also well seen in the corresponding HAADF images (see Fig. 3 f, g). The positions of the Mn atoms in the $Al_{78}Mn_{17.5}Pt_{4.5}$ R-phase and T-phase, projected along the [001] direction build the above-mentioned flattened hexagons and occupy the positions inside the central rhombi of the basic structure, while in $Al_{78}Mn_{17.5}Pt_{4.5}$ the central eight Mn atoms are replaced by Pt (see Fig. 3) and neither partial nor mixed occupancies are suggested.

The earlier published structural models of the T-phase, containing mixed occupation of several sites, were constructed for lower-Al concentrations (see points #5 to 7 in Fig. 1b): $Al_{74.6}Mn_{25.4}$ [22a], $Al_{73.3}Mn_{22.7}Pd_{4.0}$ [17b], $Al_{72.3}Mn_{24.5}Pd_{3.2}$ [15]. Thus, in the binary model of Ref. [22a] there are only one 8d and four 4c entire Mn positions (24 Mn in total). To satisfy the suggested binary

$Al_{124}Mn_{32}$ stoichiometry, the additional eight Mn atoms are needed in the basic structure. The proper positions are occupied in [22a] by the eight Al(16) atoms, which could be replaced by Mn at the stoichiometric composition, while the remaining two 4c and two 8d Mn/Al positions could be entirely occupied by Al.

Similar arguments were applied in Ref. [15] for the model containing 113 Al, 38 Mn and 5 Pd ($Al_{72.3}Mn_{24.5}Pt_{3.2}$, see point #7 in Fig. 1b), among them there are five 8d Al/Mn atomic positions and one 8d Al/Pd position equivalent to Al(16) in [22a]. According to these authors, if the mixed Mn/Al positions were completely occupied by Al and Pd/Al by Pd, the resulting composition would be $Al_{79.5}Mn_{15.4}Pd_{5.1}$, i.e., close to the Al-rich limit of the T-phase region observed experimentally. At this composition the eight Pd atoms occupy the positions equivalent to the Pt positions in [1].

The atomic substitutions also result in the change of the space group of the T-phase [4]. The replacement of the constituent elements in the basic (stoichiometric) structures of T and R, results in their stabilization. For the T-phase forming in the Al–Mn–Pd(Pt) systems in quite wide compositional regions this could be realized according to the scheme suggested above, but in the reversed order. This should be mentioned, that in the Al-rich compounds, the Mn atoms carry negative charges due to the absorption of electrons from the structure. Therefore, with the decreasing Al concentration of the T-phase, the replacements between positively charged Al and negatively charged Mn would destabilize the structure without some opposite replacement at other positions suggested above.

4. Conclusions

- The ternary R-phase (C*mcm, a* = 7.7310 Å, *b* = 24.035 Å and *c* = 12.597 Å) is formed between 700 and 800 °C in a small compositional region around $Al_{79.5}Mn_{16}Pt_{4.5}$, belonging at 800 °C to the ternary extension of the Al–Mn T-phase.
- The stability of the Al–Mn–Pt T-phase was confirmed down to 700 °C.
- At 700 °C the R-phase is in equilibrium with the T-phase of very close composition.
- The 700 °C phase equilibria in the vicinity of the Al–Mn–Pt R-phase, also involving the ternary extensions of Al_4Pt (λ_{Pt}-phase) and Al_2Pt (β^*-phase) and the ternary χ-phase were determined.
- The atomic model of the R-phase containing 124 Al, 24 Mn and 8 Pt atoms was determined applying direct methods on the 3D ED tomography data and qualitatively verified by the HAADF TEM imaging.

Acknowledgements

The authors thank C. Thomas for technical contributions. Dr. V. Ezersky's help is deeply appreciated.

References

[1] R. Tamari, B. Grushko, L. Meshi, Structural study of $Al_{78}Mn_{17.5}Pt_{4.5}$ and (re)constitution of the Al–Mn–Pt system in its vicinity. J. Alloys Comp. 861 (2021) 158328. https://doi.org/10.1016/j.jallcom.2020.158328.

[2] B. Grushko, A study of the Al–Mn–Pt alloy system, J. Alloys Comp. 792 (2019) 1223-1229. https://doi.org/10.1016/j.jallcom.2019.04.130.

[3] S. Balanetskyy, G. Meisterernst, M. Heggen, M. Feuerbacher, Reinvestigation of the Al–Mn–Pd alloy system in the vicinity of the T- and R-phases, Intermetallics 16(1) (2008) 71-87. https://doi.org/10.1016/j.intermet.2007.08.002.
[4] R. Tamari, B. Grushko, L. Meshi, Electron diffraction study of the space group variation in the Al–Mn–Pt T-phase, Symmetry 14 (2022) 38. https://doi.org/10.3390/sym14010038
[5] a) L. Palatinus, PETS: program for analysis of electron diffraction data, Inst. Phys. Czech Acad. Sci. (2011).
b) Triple commercial software http://www.calidris-em.com/triple.php
[6] M.C. Burla, R. Caliandro, M. Camalli, B. Carrozzini, G.L. Cascarano, L. De Caro, R. Spagna, Il Milione: a suite of computer programs for crystal structure solution of proteins, J. Appl. Cryst. 40 (3) (2007) 609–613. https://doi.org/10.1107/ S0021889807010941.
[7] G.M. Sheldrick, SHELXL-97, Program for Crystal Structure Refinement, University of Goettingen, Germany, 1997.
[8] M. Boudard, Structural themes in approximant and decagonal quasicrystalline phases in Al based alloys. J. Alloys Comp. 495 (2010) 365-371.
https://doi.org/10.1016/j.jallcom.2009.10.063.
[9] K. Robinson, The unit cell and Brillouin zones of $Ni_4Mn_{11}Al_{60}$ and belated compounds. Phil. Mag. 43 (1952) 775-782. DOI: 10.1080/14786440708520993
[10] K. Robinson, The determination of the crystal structure of $Ni_4Mn_{11}Al_{60}$, Acta Cryst. 7 (1954) 494-497. https://doi.org/10.1107/S0365110X54001570.
[11] A. Damjanovic, The structure analysis of the T_3(AlMnZn) compound. Acta Cryst. 14 (1961) 982-987.
[12] a) B. Grushko, D. Pavlyuchkov, S.B. Mi, S. Balanetskyy, Ternary phases forming adjacent to Al_3Mn-Al_4Mn in Al–Mn–TM (TM = Fe, Co, Ni, Cu, Zn, Pd). J. Alloys Comp. 677 (2016) 148-162.
b) B. Grushko, S. Mi, Al-rich region of Al–Cu–Mn, J. Alloys Comp. 688 (2016) 957-963. http://dx.doi.org/10.1016/j.jallcom.2016.07.075.
[13] S. Balanetskyy, G. Meisterernst, B. Grushko, M. Feuerbacher, The Al-rich region of the Al-Mn-Ni alloy system. Part II: Phase equilibria at 620 – 1000 °C. J. Alloys Comp. 509 (2011) 3795-3805. https://doi:10.1016/j.jallcom.2010.10.114
[14] T. Hahn, International Tables for Crystallography, volume A: space-group symmetry, 5th ed., Springer, (2002) 48.
[15] H. Klein, M. Boudard, M. Audier, M. de Boissieu, H. Vincent, L. Beraha, M. Duneau, The T-Al_3(Mn, Pd) quasicrystalline approximant: chemical order and phason defects, Phil. Mag. Let. 75(4) (1997) 197-208.? https://doi.org/10.1080/095008397179624.
[16] Zhenju Shen, Chunhui Liu, Qingqing Ding, Shuangbao Wang, Xiao Wei, Lu Chen, Jixue Li, Ze Zhang, The structure determination of $Al_{20}Cu_2Mn_3$ by near atomic resolution chemical mapping. J. Alloys Comp. 601 (2014) 25-30. http://dx.doi.org/j.jallcom.2014.02.125.
[17] M. Gemmi, A.E. Lanza, 3D electron diffraction techniques, Acta Cryst B 75 (4) (2019) 495-504, https://doi.org/10.1107/S2052520619007510
[18] L. Meshi, S. Samuha, "Characterization of atomic structures of nanosized intermetallic compounds using electron diffraction methods", Advanced Materials 30 (41) 1706704 (2018)
[19] H. Klein, J. David, The quality of precession electron diffraction data is higher than necessary for structure solution of unknown crystalline phases, Acta Cryst A67 (2011) 297-302, https://doi.org/10.1107/S0108767311006581

[20] S.J. Sedlmaier, E. Mugnaioli, O. Oeckler, U. Kolb, W. Schnick, SrP2N5O: a highly condensed layer phosphate structure solved from a nanocrystal by automated electron diffraction tomography, Chemistry 17 (40) (2011) 11258-65, doi: 10.1002/chem.201101545
[21] G. Yaniv G., L. Meshi, Structure characterization of novel alluminides in the Nd-Re-Al system by electron crystallography methods", Materials Characterization 168 (2020) 110562
[22] (a) K. Hiraga, M. Kaneko, Y. Matsuo, S. Hashimoto, The structure of Al_3Mn: close relationship to decagonal quasicrystals, Phil. Mag. B67 (2) (1993) 193–205, https://doi.org/10.1080/13642819308207867.
(b) Y. Matsuo, M. Kaneko, T. Yamanoi, N. Kaji, K. Sugiyama, K. Hiraga, The structure of an Al_3Mn-type Al_3(Mn, Pd) crystal studied by single-crystal X-ray diffraction analysis, Phil. Mag. Let. 76(5) (1997) 357-362. https://doi.org/10.1080/095008397178968.

Figure captions

Fig. 1. Phase equilibria in the vicinity of the R-phase in Al–Mn–Pt at 700 °C (a), in Al–Mn–Pd at 680 °C [3] (b) and in Al–Mn–Cu at 650 °C (c) [12b]. The compositions of the studied alloys are marked in (a) by the red circles and numbered as following: #1 ($Al_{82}Mn_8Pt_{10}$), #2 ($Al_{78}Mn_{17.5}Pt_{4.5}$), #3 ($Al_{75.5}Mn_{18.5}Pt_6$) and #4 ($Al_{76}Mn_{22}Pt_2$). The measured compositions of the phases are marked by open squares. No compositional differences were experimentally revealed in Al–Mn–Pt between the coexisting phases T and R and the corresponding compositions were shown conditionally by filled squares. The provisional equilibria are shown by broken lines. The compositional regions of the T-phase are separated from the binary terminal, where this phase is only stable at 895 to 1002 °C and ~$Al_{75}Mn_{25}$-$Al_{71}Mn_{29}$. The overall ternary extensions of the T-phase are shown in orange. The $Al_{21}Pd_8$ and Al_4Pd phases, isostructural to $Al_{21}Pt_8$ and Al_4Pt respectively, are formed below 680 °C. The compositions of the Al–Mn–Pd T-phase corresponding to the structural models of Refs. [15,16] are marked in Fig. 1b as following: #5 ($Al_{74.6}Mn_{25.4}$), #6 ($Al_{73.3}Mn_{22.7}Pt_{4.0}$), #7 ($Al_{72.3}Mn_{24.5}Pt_{3.2}$). D_3 is the decagonal phase. (For the interpretation of the colors, see the online version).

Fig. 2. Small 2θ region of the powder XRD patterns (Cu Kα1 radiation) of the alloy #2 ($Al_{78}Mn_{17.5}Pt_{4.5}$) annealed at 800 °C (a) and at 700 °C (b), and that of the alloy #1 ($Al_{82}Mn_8Pt_{10}$) annealed at 700 °C (c). The y axis is in linear scale. The alloy #2 does not contain the R-phase at 800 °C, and the alloy #1 does not contain the T-phase at 700 °C, while both R and T coexist in the alloy #2 annealed at 700 °C. (For the interpretation of the colors, see the online version).

Fig. 3. Structural models of the R and T phases projected along the [001] directions (a-e) and the corresponding filtered HAADF images (f, g). The model of the $Al_{60}Mn_{11}M_4$ R-phase [10] (a), and the corresponding columns of the heavy atoms (b), the columns of the heavy atoms in the $Al_{72.3}Mn_{24.5}Pd_{3.2}$ T-phase [15] (c, corresponds to the [010] orientation in [15]), the heavy atoms in the $Al_{78}Mn_{17.5}Pt_{4.5}$ T-phase [1] (d), and in the $Al_{79.5}Mn_{16}Pt_{4.5}$ R-phase (e). Each model is shown as 2x2x2 unit cells. In (a) and (d) the unit cell edges are shown by black. The HAADF images of the $Al_{78}Mn_{17.5}Pt_{4.5}$ T-phase at 800 °C (f) and of the R-phase of the same composition at 700 °C (g). The corresponding models are overlaid the HAADF images. The scale bar is the same at both images, as shown in (g). The positions of the Mn atoms are marked by cyan, Pt and Pd/Al by red, Mn/Al by black, Al by gray and M=Ni(Cu) by green. In (a) the regular hexagons expanded along their diagonals connect the centers of the neighboring pentagons. Similar is also typical of the T-phase (not shown). The main difference between T and R arises from the different ways of linking of the corresponding pentagonal chains. Subsequently the hexagons are arranged in parallel in R and in the herringbone manner in T. (For the interpretation of the colors, see the online version).

Fig. 4. 3D reconstruction of the reciprocal space of the $Al_{79.5}Mn_{16}Pt_{4.5}$ R-phase, projections along the axes: a) [100], b) [010] and c) [001].

Fig. 5. Cuts of the reciprocal space of the $Al_{79.5}Mn_{16}Pt_{4.5}$ R-phase illustrate the deduced extinction conditions.

Table 1. Al–Mn–Pt phases mentioned in the text and diagram. The crystallographic data are reproduced from Ref. [2], apart from those of the R-phase and λ_{Pt}-$Al_{80}Mn_{3.5}Pt_{16.5}$ obtained in the present work.

Phase	Space group	Lattice parameters		
		a, Å	*b*, Å	*c*, Å
		α, °	*β*, °	*γ*, °
λ_{Pt}-$Al_{80}Pt_{20}$	P3*c*1	13.089	-	9.633
λ_{Pt}-$Al_{80}Mn_{3.5}Pt_{16.5}$		13.0423(7)	-	9.6587(9)
$Al_{21}Pt_8$	I4$_1$/*a*	12.942	-	10.659
β*-Al_2Pt	$Fm\bar{3}m$	5.9194	-	-
Al_6Mn	C*mcm*	7.5551	6.4994	8.8724
μ_{Mn}-Al_4Mn	P6$_3$/*mmc*	20.015	-	24.699
T-$Al_{72.8}Mn_{27.2}$	P*nma*	14.873	12.420	12.547
T-$Al_{78}Mn_{17.5}Pt_{4.5}$	P*na*2$_1$	14.720	12.628	12.545
ν_{Mn}-$Al_{11}Mn_4$	P$\bar{1}$	5.095	8.879	5.051
		89.35	100.47	105.08
χ	P31*c*	12.207	-	27.248
R	C*mcm*	7.730(2)	24.035(6)	12.593(3)

Table 2. Atomic parameters for the $Al_{79.5}Mn_{16}Pt_{4.5}$ R-phase. The thermal displacement parameters U of Al were treated as isotropic, of Mn and Pt Al as anisotropic (their equivalent U are marked by asterisk).

Atom	Wyckoff position	x	y	z	U
Pt1	8f	0.0000	0.0849(3)	0.5716(4)	0.0084*
Mn1	4c	-0.5000	0.0491(0)	0.7500	0.5469*
Mn2	8g	-0.3207(3)	0.2147(7)	0.7500	0.0147*
Mn3	8f	-0.5000	0.1328(6)	0.4441(0)	0.0650*
Mn4	4c	0.0000	0.0559(2)	0.2500	0.6575*
Al1	16h	-0.6531(4)	0.0485(3)	0.6121(1)	0.1468
Al2	16h	-0.1951(0)	0.1703(4)	0.5270(2)	0.0247
Al3	16h	-0.1356(0)	0.2980(9)	0.6510(6)	0.1343
Al4	8g	-0.2386(2)	-0.0084(4)	0.7500	0.0058
Al5	16h	-0.2010(8)	0.1126(9)	0.3792(1)	0.0045
Al6	8g	-0.1639(3)	0.0935(1)	0.7500	0.0182
Al7	8f	-0.5000	0.1457(1)	0.6374(2)	-0.0010
Al8	8f	0.0000	0.2299(0)	0.5053(4)	0.0567
Al9	4c	0.0000	0.1599(3)	0.2500	0.0848
Al10	4c	0.0000	0.2033(2)	0.7500	0.0349
Al11	8f	-0.5000	0.0435(3)	0.3730(0)	0.0246
Al12	4c	-0.5000	0.1316(0)	0.2500	0.0189
Al13	8f	0.0000	0.0149(6)	0.4171(5)	-0.0010

Table 3. Interatomic distances (in Å) between the heavy atoms and neighboring (first coordination) atoms in the $Al_{79.5}Mn_{16}Pt_{4.5}$ R-phase.

Coordination of Pt	Coordination of Mn1	Coordination of Mn2	Coordination of Mn3	Coordination of Mn4
Al13 2.40	4xAl1 2.10	Al10 2.49	2xAl3 2.30	2xAl4 2.17
Al13 2.57	2xAl4 2.45	2xAl7 2.59	Al11 2.33	2xAl13 2.32
2xAl6 2.59	2xAl11 2.71	2xAl3 2.76	Al12 2.44	Al13 2.32
2xAl2 2.61	2xAl7 2.72	Mn2 2.77	Al7 2.46	Al9 2.50
2xAl1 2.87	2xAl6 2.81		2xAl5 2.50	4xAl5 2.63
2xAl5 2.96			2xAl2 2.73	

Table 4. Absolute distances (AD) between the equivalent atomic positions in the $Al_{79.5}Mn_{16}Pt_{4.5}$ R-phase and in the model of Ref. [10].

Corresponding Wyckoff position	Al-Mn-Pt R-phase model [current work]	Al-Mn-Ni R-phase model [10]	Distances between the corresponding atom positions, [Å]
8f	Pt1	Mn4	0.0665
4c	Mn1	Mn1	0.1678
8g	Mn2	Ni1	0.0139
8f	Mn3	Mn3	0.1464
4c	Mn4	Mn2	0.5731
16h	Al1	Al1	0.6536
16h	Al2	Al2	0.4775
16h	Al3	Al3	0.5851
8g	Al4	Al4	0.2800
16h	Al5	Al5	0.1665
8g	Al6	Al6	0.3370
8f	Al7	Al7	0.2390
8f	Al8	Al8	1.1375
4c	Al9	Al9	0.6443
4c	Al10	Al10	0.0080
8f	Al11	Al11	0.1457
4c	Al12	Al12	0.1285
8f	Al13	Al13	0.2617

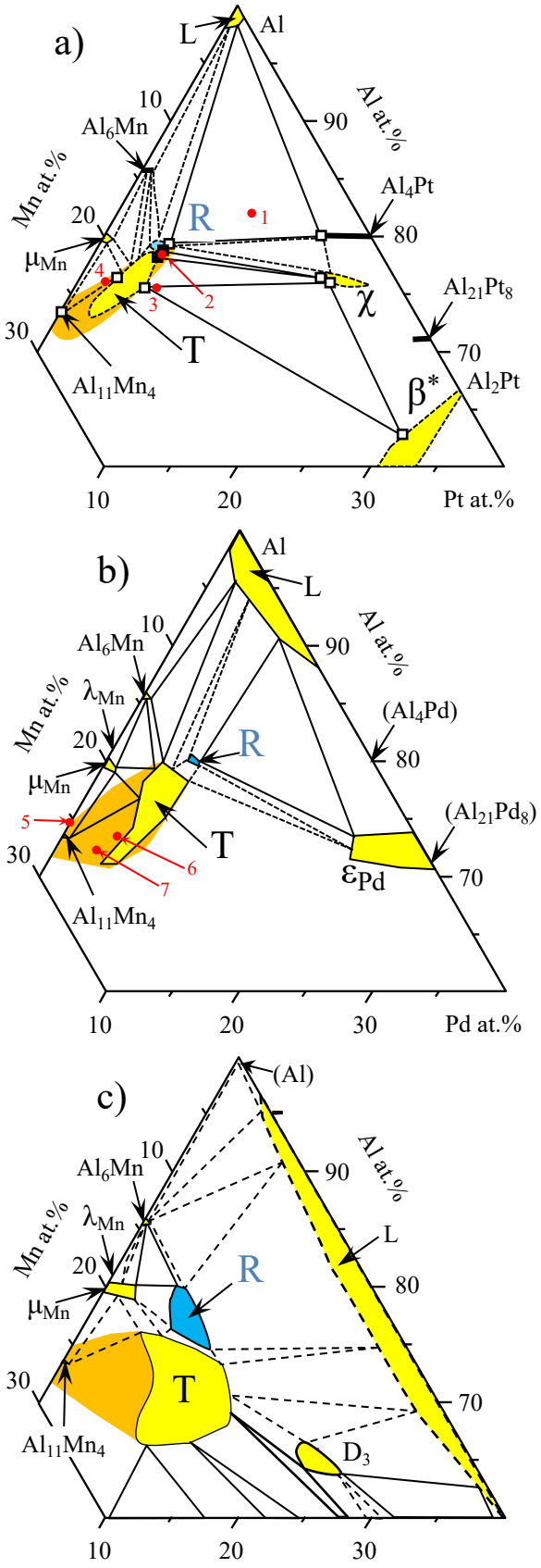
a)
L
Al
10
90
Al at.%
Al6Mn
Mn at.%
Al4Pt
20
R
1
80
μMn
4
2
3
χ
Al21Pt8
30
70
T
Al2Pt
Al11Mn4
β*
10
20
30
Pt at.%
b)
Al
L
10
90
Al at.%
Al6Mn
λMn
(Al4Pd)
Mn at.%
20
R
80
μMn
5
(Al21Pd8)
T
30
6
7
εPd
70
Al11Mn4
10
20
30
Pd at.%
c)
(Al)
10
90
Al at.%
Al6Mn
λMn
L
Mn at.%
20
R
80
μMn
30
T
70
Al11Mn4
D3
10
20
30

Fig. 1

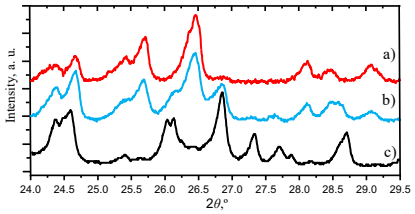
Intensity, a. u.
a)
b)
c)
24.0 24.5 25.0 25.5 26.0 26.5 27.0 27.5 28.0 28.5 29.0 29.5
2θ,°

Fig. 2

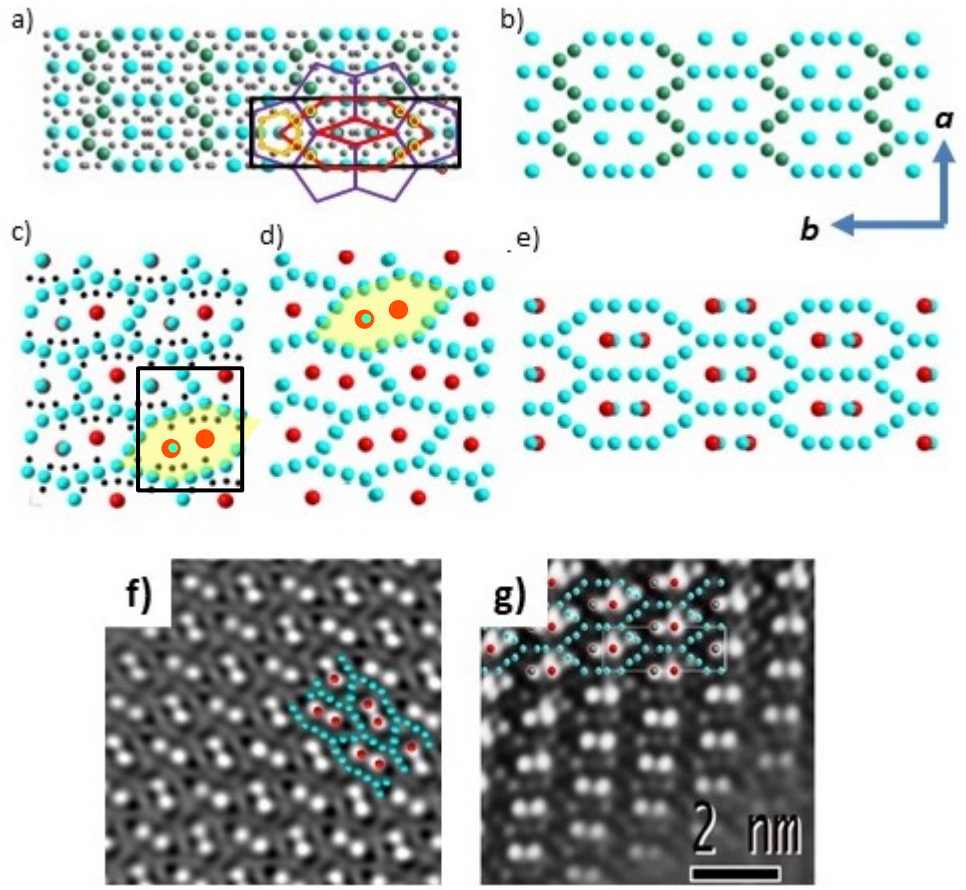
a)
b)
a
b
c)
d)
e)
f)
g)
2 nm

Fig. 3

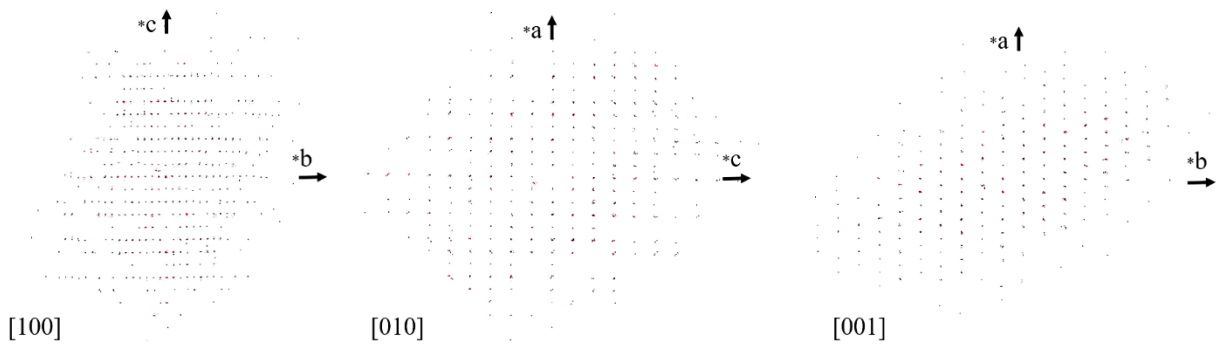

Fig. 4

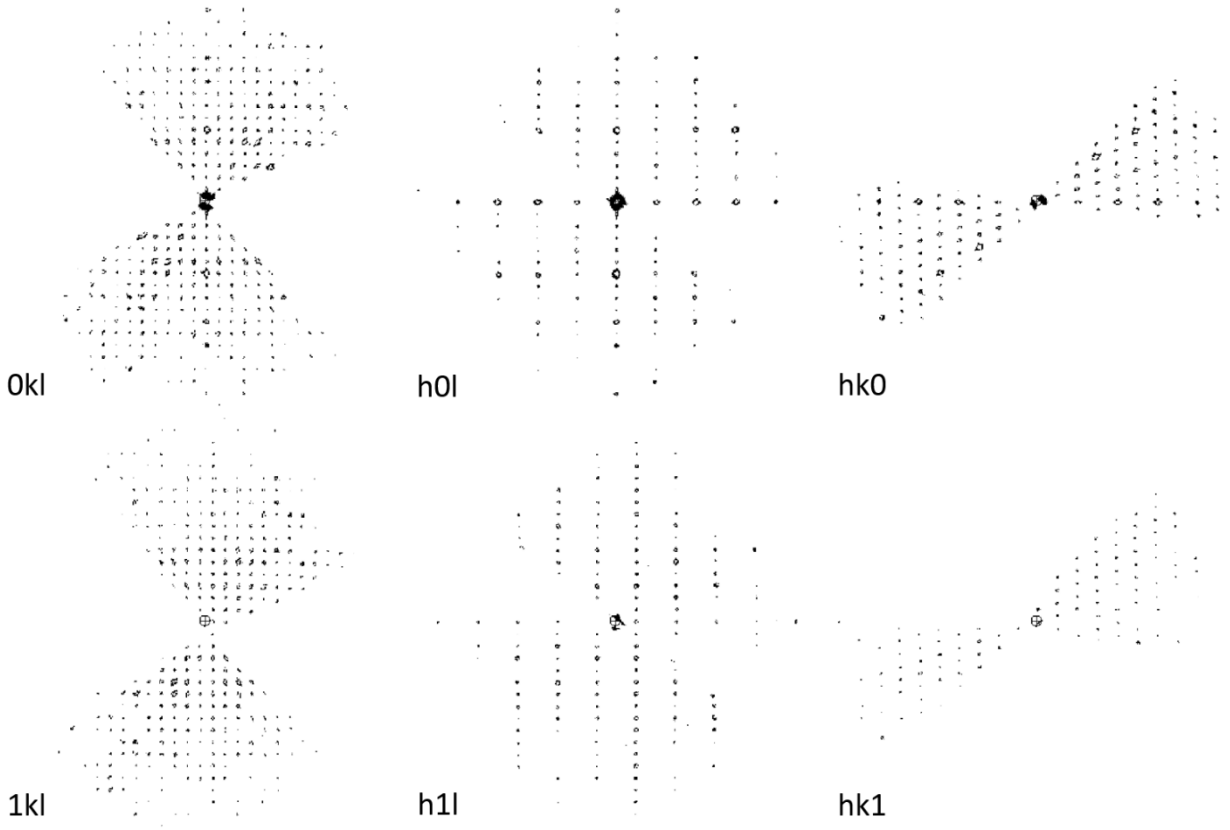

Fig. 5